Progress In Electromagnetics Research, Vol. 137, 439–452, 2013

USE OF ALIGNED CARBON NANOTUBES AS ELECTRIC FIELD SENSORS

Chieh-Lien Lu[1], Hsin-Jung Tsai[1], Bee-Yu Wei[2], and Wen-Kuang Hsu[1, *]

[1]Department of Materials Science and Engineering, National Tsing Hua University, Hsinchu, Taiwan

[2]Chemistry & Materials Research Laboratory, Industrial Technology Research Institute, Hsinchu, Taiwan

Abstract—Application of electric field in normal to aligned carbon nanotubes creates Coulomb forces at intertube junctions and tubes become closely packed. Packed structure facilitates intertube transfer of carriers and reduced resistance is found to scale with field strength. Aggregated nanotubes are therefore used as field sensors and sensitivity is evident by drastic fluctuations of resistance. Sensing mechanism is discussed and verified.

1. INTRODUCTION

Carbon nanotubes (CNTs) are one dimension conductor made of rounded graphene sheets and conjugated networks endows such a seamless structure with electronic stability and mechanical strength [1]. For example, CNTs do not suffer from the peierls distortion at low temperature and remain electrically conductive at stressed forms [2]. Upon bending, stresses can be rapidly dispersed through rigid networks and tubes buckle to prevent bond breaking at bends [3]. Study also reveals that transport through individual tubes is governed by band structure near to the Fermi level (E_F) and conductance can be modulated with a gate electrode at both negative and positive fields [4]. Conduction however changes from diffusive to hopping mode as nanotubes aggregate and hopping range is controlled by Boltzmann energy (k_BT) [5]. At high temperature, carriers hop simultaneously along transverse and longitudinal directions and tube

Received 17 January 2013, Accepted 22 February 2013, Scheduled 28 February 2013

* Corresponding author: Wen-Kuang Hsu (wkhsu@mx.nthu.edu.tw).

resistance (R) is determined by structure factors, including aspect ratio and degree of graphitization [6]. Transfer is restricted as temperature decreases and R arises mainly from intertube barrier (E_a). Previous workers have discovered that E_a can be reduced by electrolyte addition and chemical treatments; the former results in intercalation of coordinated cations and provides low energy passages between tubes [5]. Chemical treatments produce dipolar defects and reduced E_a is owing to preferential hopping through oxygenated lattices and dangling edges [7]. In this work, conductance of aggregated multi-walled CNTs (MWCNTs) is probed in the presence of electric field (E) and a correlation is observed between E_a change and E direction. When E is applied in parallel with tubes (E_{ll}) transport remains unaffected and E_a change is very small. The R decreases however noticeably as tubes are arranged in normal to E ($E_{\perp}$) and reduced E_a is verified as a result of Coulomb force (F_C) assisted transfer at intertube junctions. In vacuum, F_C is enhanced and R decease is amplified. Aligned CNTs are then used as E sensor and R strongly fluctuates in response to ac E. Study also reveals at ambient condition that tubes tend to bundle and alignment enhanced intertube binding is verified by experiments and *ab-initio* calculations.

2. EXPERIMENTAL

CNT-sensors are made according to procedures as follows. First, a silicon wafer (30×30 mm) is placed in an electrical furnace and alumina tube is repeatedly purged with N_2 at 300°C. Second, the furnace temperature is raised to 850°C and ferrocene dissolved xylene solution (0.02 g/10 c.c.) is injected into ceramic tube. This produces arrays of aligned MWCNTs on silicon substrate [8] and array height is measured to be 1 ± 0.01 mm, corresponding to 30–35 tubes connected in head-to-end fashion (Figures 1(a)–(b)). Third, CNT arrays are carefully

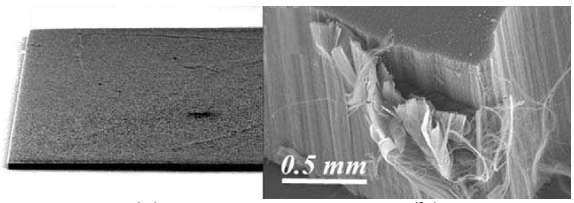

Figure 1. SEM images of aligned MWCNTs at (a) low and (b) high magnifications.

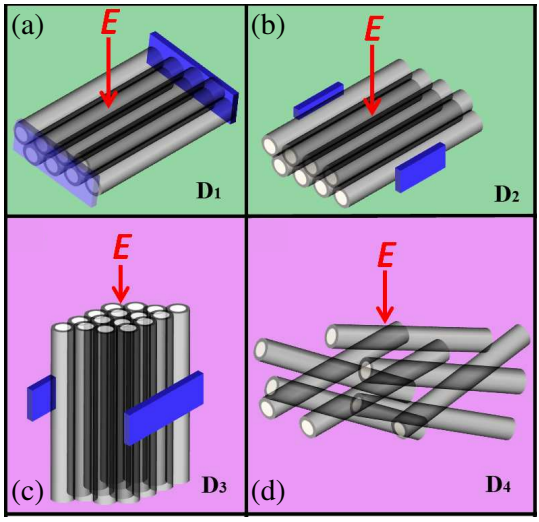

Figure 2. CNTs-$\mathbf{E}_{con}$ configurations of (a) $\mathbf{D}_1$, (b) $\mathbf{D}_2$, (c) $\mathbf{D}_3$ and (d) $\mathbf{D}_4$.

peeled off from substrate and are sliced into stripes ($2 \times 2 \times 0.3$ mm). Four different devices are fabricated and are hereafter defined as $\mathbf{D}_1$, $\mathbf{D}_2$, $\mathbf{D}_3$ and $\mathbf{D}_4$, respectively. In $\mathbf{D}_1$ and $\mathbf{D}_2$, tubes are arranged at $E_\perp$ and silver paste is painted respectively to strip-ends and -sides as electrical connections ($\mathbf{E}_{con}$) (Figures 2(a), (b). Tubes in $\mathbf{D}_3$ are arranged at E_{ll} and R is measured along c-axis (Figure 2(c)). $\mathbf{D}_4$ consists of dispersed tubes between $\mathbf{E}_{con}$ and is made for a comparison (Figure 2(d)). Electrical measurements are carried out using a two-terminal technique and R changes are in-situ recorded by a Keithly-2400 power supply with background noise controlled at ± 0.5 nA. The charge density is calculated according to *ab-initio* method and procedures are briefed as follows. A semiconducting tube (5, 0) is built in a $1 \times 1 \times 1$ nm frame and structure is relaxed to a minimal potential. The density functional theory is treated with exchange-correlation and Perdew-Ultrasoft pseudo-potentials, and self-consistent field tolerance threshold is set at 10^{-6} eV/atom for structural convergence and 0.05/Å for Monkhorst-Pack k-point grid separation. An E ($= 0.06$ mV/Å) is applied vertically to tube and charge density is measured with a standard k-point path method [9].

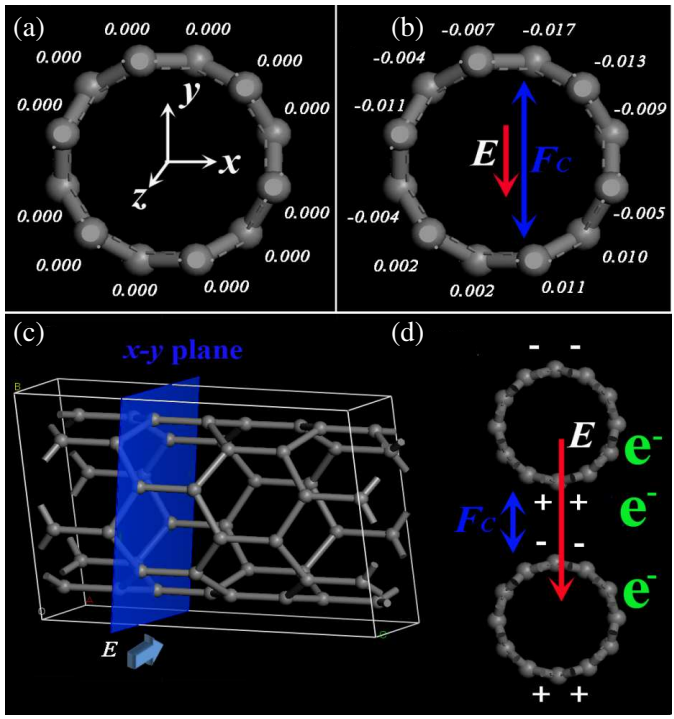

Figure 3. A simulated (5, 0) semiconducting tube at (a) $E = 0$, (b) $E = 0.06\,\mathrm{mV/\AA}$, (c) side view of stressed x-y plane (blue), and (d) F_C creation at intertube channel.

3. RESULTS AND DISCUSSION

At $E_\perp = 0$, chemical potential at each atom is identical and charge distribution is uniform (Figure 3(a)). Tube however becomes polarized at $E_\perp = 0.06\,\mathrm{mV/\AA}$ and the negative and positive charges locate at top and bottom surfaces respectively, forming a dipolar shell (Figure 3(b)). The E induced F_C however creates shell stresses (σ) and σ at x-, y- and z-axes are found to be $\sigma_x = -14.02\,\mathrm{GPa}$, $\sigma_y = -14.40\,\mathrm{GPa}$ and $\sigma_z = -10.43\,\mathrm{GPa}$: the $\sigma_x \sim \sigma_y > \sigma_z$ indicates compression along E direction (Table 1 & blue, Figure 3(c)). Simulation carried out on two tubes arranged in parallel yield a similar result whereas F_C shifts to intertube channel and causes a decrease in tube-tube spacing (Figure 3(d)). Figure 4(a) displays hexagonally packed CNTs in a $5 \times 5 \times 5\,\mathrm{nm}$ potential cell and tube-tube correlation is geometrically optimized. At $E_\perp = 0$, σ approximates zero and tubes are spaced

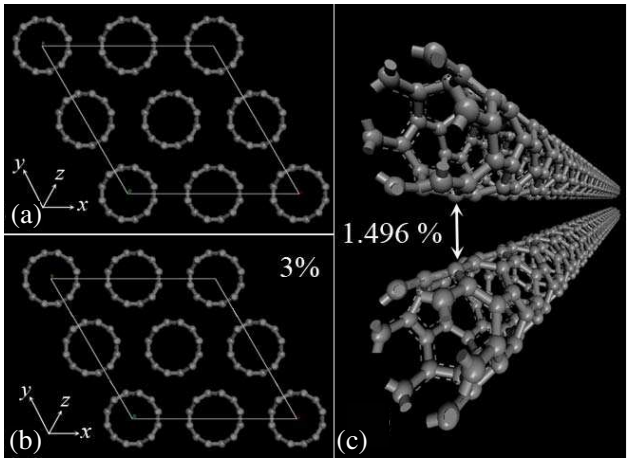

Figure 4. Hexagonally packed tubes at (a) $E = 0$, (b) $0.06\,\mathrm{mV/\AA}$ and (c) reduced intertube separation.

by a distance corresponding to the van der Waal's interaction. Cell however contracts by 3% at $E_{\perp} = 0.06\,\mathrm{mV/\AA}$ (Figure 4(b)) and intertube separation is reduced by 1.496% (Figure 4(c)), consistent with Figure 3(d). According to variable-hopping range model, the E_a at a given temperature (T) is a function of intertube-spacing (T) and decreases as tubes are pressed [10–12]. Here we find that E_a truly decreases with F_C creation and is supported by R reductions at $E_{\perp} \neq 0$. Figure 5(a) displays E *vs.* specific resistance (R/R_o) profiles obtained from $\mathbf{D}_1$ and, the red and blue arrows represent data recording at $E \neq 0$ and 0 respectively. At $E = 0.02 - 0.08\,\mathrm{mV/\AA}$, the R/R_o variation is indistinguishable and profile fit with baseline at $E = 0.1\,\mathrm{mV/\AA}$ reveals a 0.001% decrease only. The R/R_o decrease in $\mathbf{D}_2$, in contrast, is significant and scales with E strength. For example, the R/R_o reduction is 0.102% at $E = 0.02\,\mathrm{mV/\AA}$ and reaches 0.307% at $E = 0.04\,\mathrm{mV/\AA}$, 0.562% at $0.06\,\mathrm{mV/\AA}$, 0.716% at $0.08\,\mathrm{mV/\AA}$ and 0.766% at $0.10\,\mathrm{mV/\AA}$ (Figure 5(b)). According to electrical percolation theory the equivalent circuits of current devices can be expressed as $R = \sum R_n + \sum 1/R_n + R_{con}$ where $\sum R_n$ and $\sum 1/R_n$ denote CNT resistors connected in series and parallel and do not change with E application. The R_{con} is resistance arising from intertube contacts, corresponding to E_a [6, 13]. For $\mathbf{D}_1$, R is dominated by $\sum R_n$ and $\sum 1/R_n$ and is less affected by E, accounting for infinitesimal decrease in Figure 5(a). R in $\mathbf{D}_2$ mainly arises from R_{con} and therefore varies

Table 1. $E_\perp$ created σ in a (5, 0) tube.

Stress Tensor (GPa)			
	σ_x	σ_y	σ_z
σ_x	−14.02695	−0.33095	−0.000001
σ_y	−0.33095	−14.408738	−0.000001
σ_z	−0.000001	−0.000001	−10.429164
Total Pressure: 12.9548			

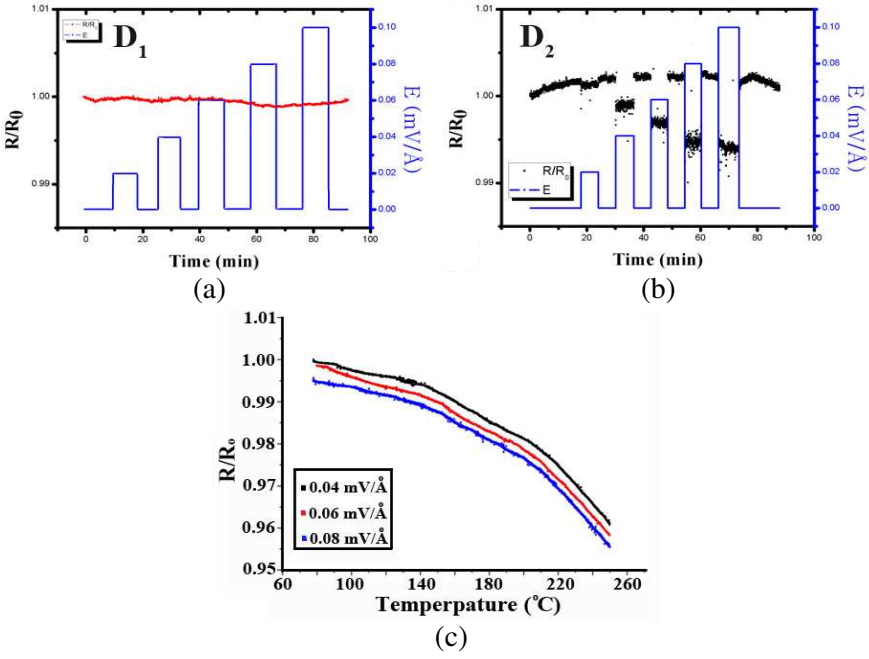

Figure 5. The R/R_o-E plots of (a) $\mathbf{D}_1$, (b) $\mathbf{D}_2$, and (c) R/R_o-T plots of $\mathbf{D}_2$.

significantly with E. Accordingly, R/R_o decrease in Figure 5(b) must originate from reduced R_{con} and R_{con}-governed $\mathbf{D}_2$ is further supported by calculations based on Arrhenius plot $R = R_o \exp^{(-Ea/kBT)}$ where E_a is extracted from R/R_o profile slopes at different T (Figure 5(c)) [5]. We find that E_a decreases by 46.98×10^{-5} eV at $E = 0.04\,\text{mV/Å}$, by 50.14×10^{-5} eV at $0.06\,\text{mV/Å}$ and by 52.78×10^{-5} eV at $0.08\,\text{mV/Å}$ (Table 2), supporting E_a-E (or R-E) scaling relation.

Table 2. E_a decrease in $\mathbf{D}_2$ at various E.

$\boldsymbol{E}$ **(mV/Å)**	**0.04**	**0.06**	**0.08**
$\mathbf{E}_a$ **decrease** ($\times 10^{-5}$ **eV**)	46.98	50.14	52.78

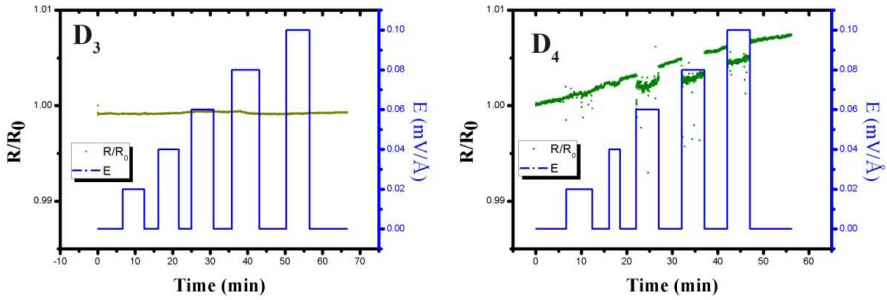

Figure 6. R/R_o-E plots of (a) $\mathbf{D}_3$ and (b) $\mathbf{D}_4$.

Transport through $\mathbf{D}_3$ also relies on intertube hopping whereas nanotubes arranged at E_{ll} cannot create an effective F_C at intertube channels and E_a-E relation is weakened, accounting for small R/R_o decrease in Figure 6(a). In fact, anisotropic effect has been observed in wave absorption experiments and absorbance reaches a maximum and minimum at $E_\perp$ and E_{ll} respectively, similar to $\mathbf{D}_3$ [14]. Additional evidence in supporting anisotropic conductance comes from $\mathbf{D}_4$ made of dispersed nanotubes between $\mathbf{E}_{con}$. In this case, circuit elements can be considered as combination of $\mathbf{D}_1 + \mathbf{D}_2 + \mathbf{D}_3$ and, R decrease is mainly contributed by R_{con}-dominated $\mathbf{D}_2$. Figure 6(b) shows $E - R/R_o$ profiles obtained from $\mathbf{D}_4$ and decrease is lower compared with Figure 3(b). For example, R is reduced only by 0.265% at $E = 0.08\,\mathrm{mV/Å}$ and by 0.355% at $0.10\,\mathrm{mV/Å}$. Experiments however were carried out in ambient condition and F_C may, to some extent, be compromised by intercalated O_2 molecules [15]. We have tested $\mathbf{D}_2$ in vacuum at 300 K (a) and 77 K (b), and recorded data is compared with Figure 5(b) ((c), Table 3). At 300 K, R/R_o decreases by 0.237% at $E = 0.02\,\mathrm{mV/Å}$ and by 0.478% at $0.04\,\mathrm{mV/Å}$, greater than value seen in Figure 5(b). The R/R_o continues to decrease with E ramping and reaches 0.981% at $E = 0.1\,\mathrm{mV/Å}$, indicative of F_C enhancement upon air removal. At $T = 77\,\mathrm{K}$, R decrement is further

Table 3. $E_\perp$ induced R/R_o decrease in vacuum (10^{-3} torr) at 300 K (a) and 77 K (b), and comparison with data recorded at ambient condition (c). Sample: $\mathbf{D}_2$. Units: E (mV/Å), and R/R_o decrease (%).

E	**0.02**	**0.04**	**0.06**	**0.08**	**0.10**
(a)	0.237	0.478	0.852	0.943	0.981
(b)	0.55	1.109	1.658	2.016	2.493
(c)	0.102	0.307	0.562	0.716	0.766

amplified and measurements give 0.55% at $E = 0.02$ mV/Å, 1.109% at 0.02 mV/Å, 1.658% at 0.02 mV/Å, 2.016% at 0.02 mV/Å and 2.494% at 0.02 mV/Å. Origin of large R decrease at low T from Luttinger instability ($T^{0.46}$) is unlikely because carriers do not electronically correlate in hopping processes and Figure 5(c) fit with power law yields $T^{0.15-0.22}$ [7]. According to Arrhenius equation R decrease is determined by the Boltzmann factor [$\exp^{(-Ea/kBT)}$] and becomes significant as E_a exceeds k_BT. Calculation based on Figure 5(c) gives $E_a = 110$ meV and E_a/k_BT is estimated to be as high as 16 at 77 K, supporting amplification of R decrease at $E_a/k_BT \gg 1$.

E sensing technology currently relies on field-mills made of capacitive-inductive electrodes and field strength is determined according to induced current magnitude. Study here suggests that aligned CNTs can be used as E sensors; first, R decrease scales with E intensity (Figure 5(b) & Table 3); second, sensitivity is improved in vacuum. Figure 7(a) shows sensing profiles obtained from a high-frequency inductive furnace (insert, IGBT module power device) and $\mathbf{D}_4$ is used as sensor to evade anisotropic effect. Experiments are carried out at a distance of 10 cm away from furnace (green spot) and module power is set at 800 Hz and 1700 Hz ($\sim$ 0.02–0.05 mV/Å), similar to simulations here. In vacuum, sensing of ac E is evident by R fluctuations and variation lies on $\pm$0.7–0.75%. Fluctuation becomes relatively small as sensor is exposed to air, supporting O_2 screening effect. At 1700 Hz, R drastically fluctuates and variation is promoted to $\pm$1.8–2.1% and $\pm$1.9–2.1% in both vacuum and ambient conditions (Figure 7(b)). Fluctuation vanishes as furnace is turned off and repeated experiments give a similar result (red and blue curves, Figure 7(b)). A thin foil of Al ($200 \times 200 \times 0.1$ mm) is then placed before sensor as an E shield and furnace is again switched-on. We find that E is truly shielded and R does not fluctuate (blue, Figure 5(c)). Sensing profile again re-emerges as metal foil is removed

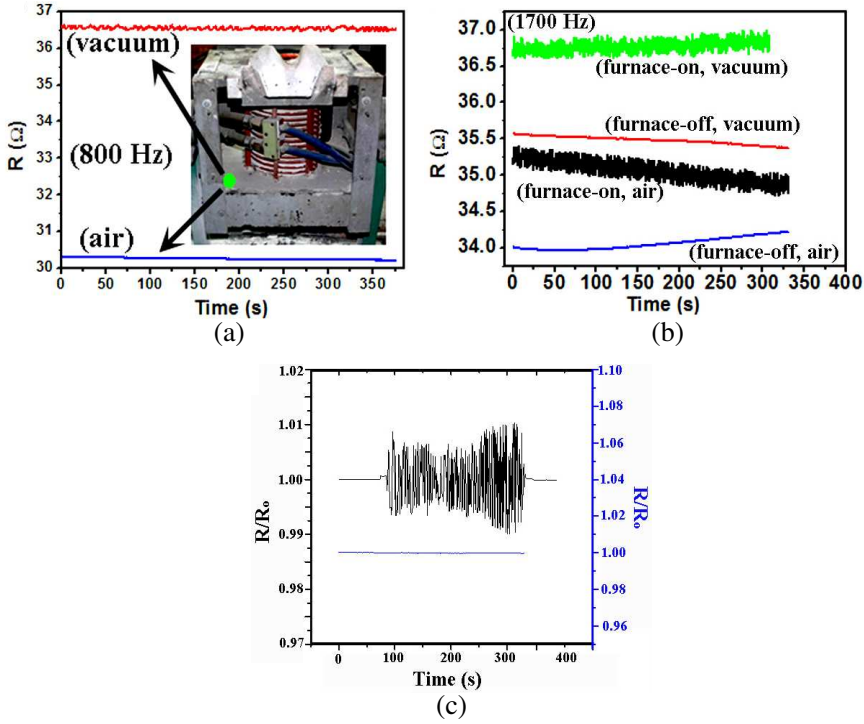

Figure 7. The real time sensing profiles obtained from a high-frequency inductive furnace at (a) 800 Hz, and at (b) 1700 Hz. Insert: side-view of inductive furnace and green spot denotes the measuring point. (c) Sensing with (blue) and without (dark) foil shielding.

and variation lies on 1–2% (dark, Figure 7(c)). Next, an infrared pyrometer is spotted onto sensor and T is found to increase only by 1°C at 800 Hz and by 2°C at 1700 Hz, excluding origin of R fluctuation from radiation induced heating [16]. It is worth mentioning that field-effect transistors made of individual tubes, in a way, resemble a sensor whereas device fabrication is time-consuming and E-controlled gating of conductance only occurs in semiconductor tubes with band-gap greater than Boltzmann energy at room T ($\sim$ 26 meV) [1]. The sensor production here is straightforward and CNTs are self-aligned. In fact, nanotubes always aggregate into bundles and alignment tendency is supported by electron microscope inspections. Figure 8 shows morphologies of MWCNTs before (a) and after a series of chemical treatments (b), including aerial oxidation at 600°C (30 min), 1200°C annealing in a vacuum (50 min) and ultrasonic dispersion (1 h,

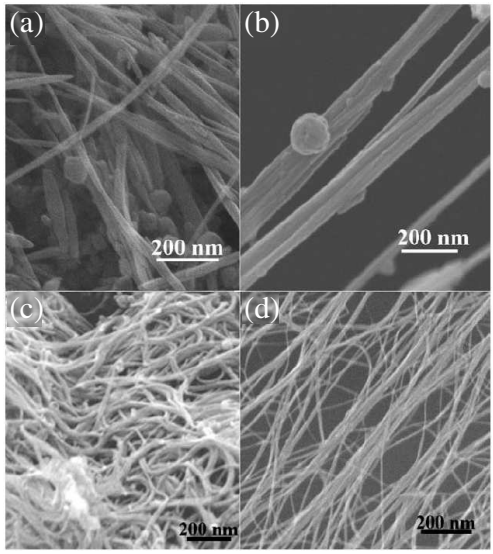

Figure 8. SEM images of (a) arc-made MWCNTs before and (b) after a series of physicochemical treatments, and (c) arc-made SWCNTs before and (d) after a series of physicochemical treatments.

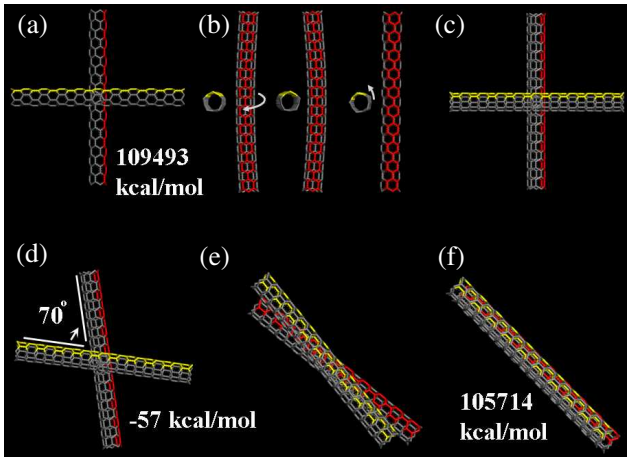

Figure 9. (a)–(f) Transitions of tube-tube correlation from crisscrossed to aligned fashions.

Clifton MU-22, 300 W). Before treatments, tubes bundle as a result of simultaneous growth, in conjunction with surface impurities created interlocking [11]. Removal of carbonaceous impurities exposes tube surfaces and re-aggregation proceeds through dispersive and dipolar forces arising from conjugated and oxygenated lattices [6, 17]. For single-walled CNTs (SWCNTs), tubes aggregate into ropes and rope dimension is estimated to be 15–25 nm in diameter and 3–5 μm in length (Figure 8(c)). Treated SWCNTs remain aggregated whereas rope dimension, possibly due to oxidative damages, is reduced to 3–6 nm and 300–600 nm (Figure 8(d)). It is worth mentioning that intertube binding has been predicted to be as weak as interlayer cohesion of graphite and lies on tens of meV, in contradiction with observations here [18]. Calculation however is based only on non-bonding energy and interactions arising from dipolar lattices are excluded. We have simulated the bundling dynamics and potential energy (E_p) of tubes at various conformations is computed according

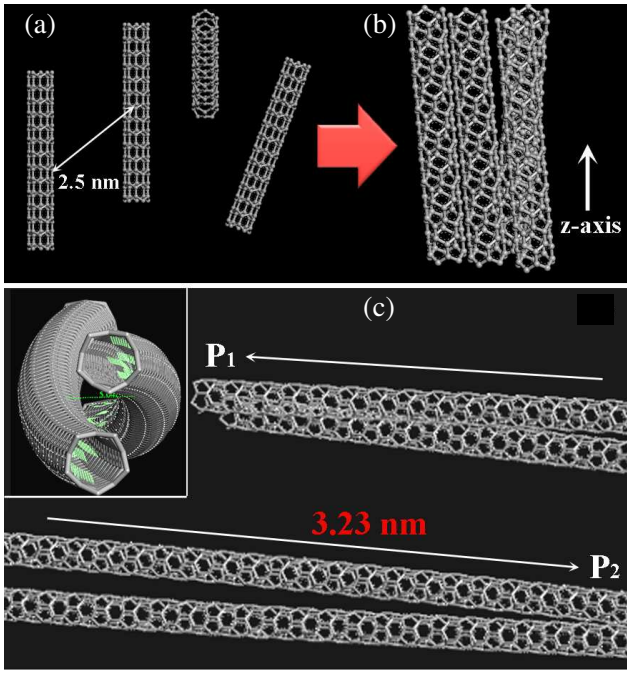

Figure 10. Bundling of (a)–(b) separated tubes, and (c) a full pitch of helicity ($P_1 \rightarrow P_2$). Insert: side-view of twisted tubes.

to *ab-initio* method [9]. Figure 9 shows transition of correlated tubes from crisscrossed ($\theta = 90°$) to aligned fashions ($\theta = 0°$) and intertube force driven alignment is realized arising from different origins. First, intertube attraction is weak at $\theta = 90°$ and tubes interact through dipolar edges (a). Tubes then slightly bend and spin to correlate (yellow/red) and registered lattices at crisscrossed point correspond to a naphthalene (b)–(c). Second, opened-edges continue to pull each other and tubes start to rotate; the E_p reduction at $\theta = 70°$ being estimated to be 57 kcal/mol (d). Third, tubes continue to rotate and intertube cohesion begins to dominate by dipole-dipole interaction arising from enhanced lattice correlation (yellow/red, (e)–(f)). Calculation gives $E_p = 109493$ kcal/mol at $\theta = 90°$ and 105714 kcal/mol at $\theta = 0°$ and reduction ($90° - 0° = 3779$ kcal/mol) is equivalent to 1.65×104 eV, comparable with reported data on parallel tubes [19]. Simulation also reveals that, if tubes are more-or-less aligned at initial stage, bundling is directly driven by intertube attraction. In this case, tubes cannot electronically correlate and E_p decrease is small (Figures 10(a), (b)).

Finally, it is worth mentioning for MWCNTs that aggregation does not cause tube winding and intertube contacts take up 5–8% of total tube surfaces [11, 20]. SWCNTs in ropes however are twisted and winding angle varies from tube to tube (Figures 8(c), (d)). Figure 10(c) shows two winding tubes and helical pitch approximates 3.23 nm ($P_1 \rightarrow P_2$, Figure 10(c)), corresponding to 5–7% increase in interface (insert, Figure 10(c)). Twisting however introduces σ into C-C networks and strain energy is calculated to be 73–80 kcal/mol, comparable with energy required for tube bending [19].

4. CONCLUSION

Isolated CNT becomes polarized at $E_\perp$ and charge separation leads to F_C formation within interior space. F_C shifts to intertube channels as tubes aggregate and results in reduced inter-spacing and E_a. Aligned tubes behave as sensor in ac E and sensitivity is evident by R fluctuations. Removal of dipolar O_2 between tubes promotes F_C and sensitivity is improved. CNTs tend to aggregate and self-alignment proceeds through multi-steps.

ACKNOWLEDGMENT

We thank the National Science Council of Taiwan for the financial support (NSC-101-2112-M-007-011-MY2).

REFERENCES

1. Dekkers, C., "Carbon nanotubes as molecular quantum wires," *Physics Today*, Vol. 52, 22–30, 1999.
2. Ebbesen, T. W., H. J. Lezec, H. Hiura, J. W. Bennett, H. F. Ghaemi, and T. Thio, "Electrical conductivity of individual carbon nanotubes," *Nature*, Vol. 382, 54–56, 1996.
3. Farajian, A. A., B. I. Yakobson, H. Mizuseki, and Y. Kawazoe, "Electronic transport through bent carbon nanotubes: Nanoelectromechanical sensors and switches," *Phys. Rev. B*, Vol. 67, 205423, 2003.
4. Appenzeller, J., J. Knoch, V. Derycke, R. Martel, S. Wind, and P. Avouris, "Field-modulated carrier transport in carbon nanotube transistors," *Phys. Rev. Lett.*, Vol. 89, 126801, 2002.
5. Li, H.-C., S.-Y. Lu, S.-H. Syue, W.-K. Hsu, and S.-C. Chang, "Conductivity enhancement of carbon nanotube composites by electrolyte addition," *Appl. Phys. Lett.*, Vol. 93, 033104, 2008.
6. Baumgartner, G., M. Carrard, L. Zuppiroli, W. Bacsa, W. A. de Heer, and L. Forró, "Hall effect and magnetoresistance of carbon nanotube films," *Phys. Rev. B*, Vol. 55, 6704–6707, 1997.
7. Lin, Y.-H., Y.-C. Lai, C.-T. Hsu, C.-J. Hu, and W.-K. Hsu, "Why aggregated carbon nanotubes exhibit low quantum efficiency," *Physical Chemistry Chemical Physics*, Vol. 13, 7149–7153, 2011.
8. Lin, Y.-H., Y.-C. Lai, C.-L. Lu, and W.-K. Hsu, "Excellent cushioning by polymer-concreted arrays of aligned carbon nanotubes," *J. Mater. Chem.*, Vol. 21, 12485, 2011.
9. Ding, J.-J., C.-L. Lu, and W.-K. Hsu, "Capacitive carbon nanotube networks in polymer composites," *Appl. Phys. Lett.*, Vol. 99, 033111, 2011.
10. Tersoff, J. and R. S. Ruoff, "Structural properties of a carbon-nanotube crystal," *Phys. Rev. Lett.*, Vol. 73, 676, 1994.
11. Syue, S.-H., C.-T. Hsu, U.-S. Chen, H.-J. Chen, W.-K. Hsu, and H.-C. Shih, "Increased strength of boron-doped carbon nanotube bundles produced by applying an electric field along their length," *Carbon*, Vol. 47, 1239, 2009.
12. Monteverde, M. and M. Núñez-Regueiro, "Pressure control of conducting channels in single-wall carbon nanotube networks," *Phys. Rev. Lett.*, Vol. 94, 235501, 2005.
13. Fischer, J. E., H. Dai, A. Thess, R. Lee, N. M. Hanjani, D. L. Dehaas, and R. E. Smalley, "Metallic resistivity in crystalline ropes of single-wall carbon nanotubes," *Phys. Rev. B*, Vol. 55,

4921–4924, 1997.

14. Chin, W., C.-L. Lu, and W.-K. Hsu, "A radiofrequency induced intra-band transition in carbon nanotubes," *Carbon*, Vol. 49, 2648–2652, 2011.
15. Collins, P. G., K. Bradley, M. Ishigami, and A. Zettl, "Extreme oxygen sensitivity of electronic properties of carbon nanotubes," *Science*, Vol. 287, 1801–1805, 2000.
16. Ramanayaka, A. N. and R. G. Mani, "Microwave-induced electron heating in the regime of radiation-induced magnetoresistance oscillations," *Phys. Rev. B*, Vol. 83, 165303, 2011.
17. Li, Y.-F., C.-I. Hung, H.-F. Kuo, S.-H. Syu, W.-K. Hsu, S.-L. Kuo, and S.-C. Huang, "Electromagnetic modulation of carbon nanotube wetting," *J. Mater. Chem.*, Vol. 19, 7694–7697, 2009.
18. Girifalco, L. A., M. Hodak, and R. S. Lee, "Carbon nanotubes, buckyballs, ropes, and a universal graphitic potential," *Phys. Rev. B*, Vol. 62, 13104–13110, 2000.
19. Syue, S.-H., S.-Y. Lu, W.-K. Hsu, and H.-C. Shih, "Internanotube friction," *Appl. Phys. Lett.*, Vol. 89, 163115, 2006.
20. Cheng, T.-W. and W.-K. Hsu, "Winding of single-walled carbon nanotube ropes: An effective load transfer," *Appl. Phys. Lett.*, Vol. 90, 123102, 2007.